




Article

Aluminum Protection by Using Green Zirconium Oxide Layer and Organic Coating: An Efficient and Adherent Dual System

Vitor B. Moreira ^{1,2} , Alvaro Meneguzzi ², Emilio Jiménez-Piqué ^{3,4}, Carlos Alemán ^{1,4} 
and Elaine Armelin ^{1,4,*} 

- ¹ Departament d'Enginyeria Química, Campus Diagonal Besòs (EEBE), Universitat Politècnica de Catalunya, 08019 Barcelona, Spain; vitor.moreira@upc.edu (V.B.M.); carlos.aleman@upc.edu (C.A.)
² Programa de Pós-graduação em Engenharia de Minas, Metalúrgica e de Materiais (PPGE3M), Universidade Federal do Rio Grande do Sul (UFRGS), Porto Alegre 91501-970, Brazil; meneguzzi@ufrgs.br
³ Department of Materials Science and Engineering, Campus Diagonal Besòs (EEBE), Universitat Politècnica de Catalunya, 08019 Barcelona, Spain; emilio.jimenez@upc.edu
⁴ Barcelona Research Center for Multiscale Science and Engineering, Campus Diagonal Besòs (EEBE), Universitat Politècnica de Catalunya, 08019 Barcelona, Spain
* Correspondence: elaine.armelin@upc.edu

Abstract: In this work, the use of ZrO₂ nanocoating in aluminum substrates, generated by controlled electrochemical chronoamperometry in hexafluorozirconic acid solutions (H₂ZrF₆·5H₂O), resulted in a lower porous films than that obtained by chemical conversion coating. After the application of an epoxy coating, long-term cyclic immersion corrosion tests and scratch tests proved the superior protection of the dual system and the coating lifespan, thanks to the enhanced adhesion of ZrO₂ intermediate layer and the organic coating. As zirconium-based electrolytes are considered more friendly bath if compared to that of other conversion coating processes, like chromating, phosphating or anodizing processes, the study opens new insights to the protection of structural metals in sectors such as automotive, naval and aerospace industries. The main advantages are the employment of lightweight intermediate pre-treatment (nanoscale), compared to conventional ones (microscale), and reduction of waste slurry (electrolyte bath free of additives).

Keywords: zirconium conversion coating; green coating; organic coating; hardness test; corrosion analysis



Citation: Moreira, V.B.; Meneguzzi, A.; Jiménez-Piqué, E.; Alemán, C.; Armelin, E. Aluminum Protection by Using Green Zirconium Oxide Layer and Organic Coating: An Efficient and Adherent Dual System. *Sustainability* **2021**, *13*, 9688. <https://doi.org/10.3390/su13179688>

Academic Editors: Ime Bassey Obot, Amrisha Singh, Akram Alfantazi and Ihsan ulhaq Toor

Received: 26 June 2021

Accepted: 23 August 2021

Published: 28 August 2021

Publisher's Note: MDPI stays neutral with regard to jurisdictional claims in published maps and institutional affiliations.



Copyright: © 2021 by the authors. Licensee MDPI, Basel, Switzerland. This article is an open access article distributed under the terms and conditions of the Creative Commons Attribution (CC BY) license (<https://creativecommons.org/licenses/by/4.0/>).

1. Introduction

The painting processes start with careful cleaning and pre-treatment of the substrate. Currently, in the technology for body car painting, common pre-treatment involves phosphating process, where the body-in-white of the vehicle is cleaned and coated with phosphate solution. The most important function of phosphate conversion coating is the adhesion promotion between galvanized body car structure and the cathodic electrodeposition primer (commonly known by KTL coating). Tricationic phosphating renders a basic level of corrosion protection and, usually, the thickness of the conversion coating is optimized by adding oxidants like molybdate, chlorate, organic nitro compounds, among other accelerators, in the phosphate bath [1]. Altogether result in a huge increase of sludge with hazardous contaminants for water effluents and elevated costs for waste recovery [2]. By other hand, since the implementation of REACH regulation in 2006 [3], chrome plating process has been eliminated as chemical passivation pretreatment in galvanized structures due to its technically proven hazardous to human health and environment [4]. Fortunately, non-phosphated zirconium-based conversion coatings are emerging as a green alternative to this conventional technology and are being considered less aggressive to the environment if compared to chromate conversion coatings and phosphating processes [5–7].

Nowadays, zirconium-based chemical conversion coatings (Zr-CCC) are the most studied pre-treatment for metal surface [8–10]. The Zr oxide layer is usually formed by

dip-coating of the metal substrates in aqueous hexafluorozirconic acid-based conversion solution (H_2ZrF_6) [6]. The resulting films are typically very thin (<100 nm) [11–14] and their composition depends on the solubility and transport of ions in the bath solution (bath agitation) [6], bath additives and pH, with zirconium oxides and hydroxides being the main components of the passivating layer [6,15–18]. For instance, Zoppas and co-workers [19] tested the efficacy of ZrO_2 obtained by dip-coating deposition (DC), as a sealing agent for aluminum anodized substrates. The samples treated with H_2ZrF_6 showed the highest corrosion resistance compared to the unsealed aluminum samples. They also applied the same strategy to galvanized steel substrates, proving that the Zr-CCC deposition is highly dependent on the solution pH and on the reaction time [20]. Such pre-treatments have demonstrated to improve both the corrosion resistance and the adhesion of top coats and adhesives [9,10,21–24]. There are several metals that were approached, such as carbon and galvanized steel [25–27], zinc [28], magnesium [29] and aluminum surfaces [13,30,31]. All them of utmost importance for the automotive and aircraft industry that strongly uses pre-treatment processes before structure protection by organic coatings.

Although good results are obtained with Zr-CCC, the zirconium electro-assisted deposition (Zr-EAD) method has come into force thanks to the excellent control over the film homogeneity and compactness [32]. The technique consists of promoting water electrolysis in the conversion bath, thus the cathodic half-reaction in acidic medium is the proton reduction reaction, leading to a pH shift on the cathode surface towards alkaline values [33–39]. In fact, the Zr-EAD deposition takes place simultaneously with the chemical conversion process driven by ions diffusion. The films are usually amorphous, which is in agreement with previous reports of similar conversion coatings produced at room temperature [34,36], and provide corrosion protection by increasing the breakdown potential of the passive layer.

2. Materials and Methods

2.1. Materials

Hexafluorozirconic acid hydrated (H_2ZrF_6 , 50% wt. in water) was supplied by Sigma-Aldrich Co. (Madrid, Spain); sodium hydroxide (pellets) was purchased from Panreac S.A. (Castellar del Vallès, Spain) and alkaline degreaser Saloclean 667N was kindly supplied by Klintex Insumos Industriais Ltda. (Cachoeirinha, Brazil). AA1100 and AA2024 plates ($5.0 \times 1.4 \times 0.3 \text{ cm}^3$) were used as substrates for Zr-DC and Zr-EAD formation in the morphological and electrochemical studies; whereas AA1100 plates ($5.0 \times 1.4 \times 0.3 \text{ cm}^3$), and AA2024 disks (3.5 cm of diameter and 4 mm of thickness) were used in the accelerated corrosion tests, in order to have a large area of analysis. The chemical composition of both substrates is supplied in the Supporting Information file (ESI). Hempadur Primer 15304 (Codes: 15308 and 95040, for epoxy base and curing agent, respectively), commercialized by Hempel S.A. (Polinyà, Spain), was used as anticorrosive organic coating.

2.2. Preparation of Aluminum Substrates for the Chemical and Electrochemical Deposition of ZrO_2

Prior the zirconium oxide deposition, the substrates were ground with silicon carbide paper from #600, down to grade #2500, to ensure similar roughness. Reproducible cleaned substrates were obtained by cleaning the surface, by one side, (i) in organic solvents and, by other, (ii) using chemical etching. The first consisted of dipping the samples in a vessel with isopropanol, followed by ethanol and, at last, acetone, at room temperature, with 5 min of time in each solvent, and using an ultrasound bath. This procedure provides a mild cleaning, aiming for the preservation of the naturally formed aluminum oxide layer (hereafter coded as “Raw”). In the second method, the samples were thoroughly washed with water and acetone, and immersed in Saloclean 667N degreasing agent (pH 9.4, 70 g/L, 70 °C) for 5 min, washed with distilled water in a sonication bath for 5 min, dried under a hot air stream, and stored under vacuum before use (hereafter coded as “Bare”). The cleaning procedure can be visualized in the Figure 1a.

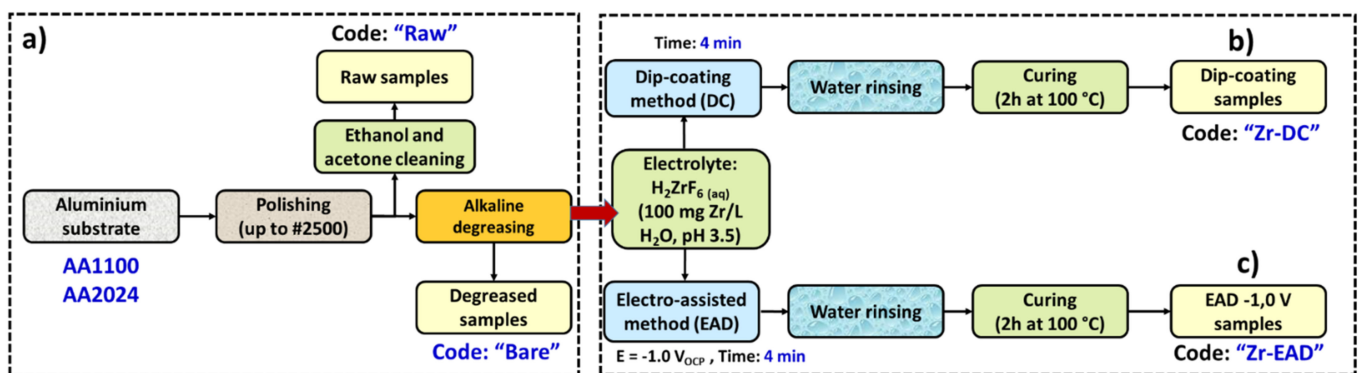


Figure 1. Flow chart for the whole processes in the preparation of the ZrO_2 nanocoating: (a) substrate polishing and cleaning steps; (b) dip-coating of aluminum substrates in H_2ZrF_6 aqueous solution; and (c) EAD in H_2ZrF_6 electrolyte, by using Al substrates as cathode.

2.3. Zirconium Chemical Conversion Coating Deposition (Zr-CCC)

The conversion bath consists of H_2ZrF_6 aqueous solution with 100 mg of Zr/L (0.015% v/v) in water. The pH was adjusted to 3.5 with a solution of NaOH 1 M. In order to produce the Zr-CCC samples (hereafter coded as “DC”, corresponding to dip-coating process), panels were immersed in the conversion solution for 4 min, followed by water rinsing and hot air stream drying before curing step for 2 h at 100 °C in a vacuum oven (Figure 1b).

2.4. Zirconium Electro-Assisted Deposition (Zr-EAD)

The Zr-EAD samples were obtained by potentiostatic electrochemical method, using the same electrolyte bath described before. The experiments were carried out in an Autolab PGSTAT302N potentiostat-galvanostat (Metrohm, Herisau, Switzerland), by using three electrodes cell, where the substrate is the working electrode with a Ag | AgCl reference electrode (3M of KCl) and graphite counter electrode. The electrolyte used in the cell is the same as used for the conversion solution. The samples were stabilized in open circuit potential (OCP) for short time (30 s) and subjected to the desired potential (−1.0 V relative to the measured OCP) during 4 min. According to this procedure, the samples generated were named as “EAD”. Samples coated by EAD method were further post-treated for 2 h at 100 °C, in a vacuum oven, to achieve a good compactness of oxide layer and reduction of defects (Figure 1c), i.e., the same post-treatment operated with DC samples (Section 2.3). The film topography and the cross-section thicknesses were measured by scanning electron microscopy (SEM), with a Focus Ion Beam (FIB) Zeiss Neon 40 instrument (Carl Zeiss, Oberkochen, Germany). The samples were previously coated with a sputtered carbon layer and received a thin protective layer of platinum (gas injection) before surface cutting. An electron beam of 5 kV was applied and the thickness of each sample was evaluated after 50 measurements, using high magnification images.

2.5. Electrochemical Characterization of Zirconium Oxide Layer

The experiments were performed in an Autolab PGSTAT302N potentiostat-galvanostat (Metrohm, Herisau, Switzerland) equipment. The electrochemical cell consisted of three electrodes, having the sample set as the working electrode, a platinum wire as counter electrode and a Ag | AgCl (KCl, 3M) as reference electrode. The tested area was 0.785 cm² and the electrolyte used in both potentiodynamic polarization and electrochemical impedance spectroscopy (EIS) tests was an aqueous 0.05 M NaCl solution. The curves were registered after 30 min of open circuit potential (OCP) stabilization.

In the potentiodynamic study (polarization tests), the potential sweep ranged from −0.3 V_{OCP} to +1.0 V_{OCP} with a scan rate of 1 mV/s. The run times for each experiment were: 24 h (1 day), 48 h (2 days), 96 h (5 days) and 168 h (7 days).

EIS experiments were also performed to evaluate the stability of the ZrO₂ nanocoating, as a function of time exposure to the electrolyte solution. The amplitude of the EIS perturbation signal was 10 mV/peak, the frequency ranged from 10⁵ to 10⁻¹ Hz taking measurements of 10 frequencies per decade. The same run times as that used in the polarization tests were approached. The Randles circuit [$R_s \cdot (R_p \cdot CPE_{dl})$] was applied to get the electrochemical parameters expressed in the Results and Discussion section.

The coating porosity (P), after the metal bare pre-treatment with alkaline degreasing solution and after the formation of zirconium oxide coating, was evaluated following the procedure described by previous authors (Equation (1)) [2,40,41]:

$$P = \frac{R'_p}{R_p} \times 10^{-(\Delta E_{\text{corr}}/\beta_a)} \times 100 \quad (1)$$

where, R'_p and R_p are the polarization resistance of Raw and coated substrates, respectively; ΔE_{corr} is the corrosion potential difference between the Raw substrate and the coated substrates, and β_a is the anodic Tafel coefficient of bare substrate, obtained in the potentiodynamic anodic polarization study. Polarization resistance was calculated from parameters obtained with the Tafel extrapolation method, using Nova 2.1 software. Those parameters were taken after 24 h of immersion in NaCl 0.05 M, to ensure the OCP stabilization for both aluminum substrates.

2.6. Organic Coating Deposition, Accelerated Corrosion Assays and Scratch Resistance

The primer used as a second coating layer for the protection of AA1100 and AA2024 surfaces is a commercial polyamide cured anticorrosive epoxy primer, two-components, containing zinc phosphate as a corrosion inhibiting pigment. This primer is characterized by a high performance in protection against corrosion and the dry film paint has good mechanical properties. Therefore, the aim of this study is to certify the adherence properties of the samples electrochemically treated, i.e., with the ZrO₂ nanocoating generated by EAD method, compared to the degreased samples (Bare), under a long period of exposition in a corrosive medium.

The resin-hardener ratio (v/v) (Hempadur 15308 and curing agent 95040) used was 4/1, according to the manufacturer recommendations (Pinturas Hempel S.A., Polinyà, Spain). The mixture was prepared in a polyethylene reservoir at room temperature (25 °C) by stirring it for about 15 min. The specimens, properly treated (Sections 2.2 and 2.4), were manually painted using a paint roller. Afterwards, all the painted specimens were allowed to cure for 7 days at room temperature in a fume hood. The edges and holes were additionally protected with impermeable polyester tapes (Polyester tape 8992, 3M Company, Madrid, Spain) to avoid corrosion. Once the paint was completely dried, thickness was measured by using Mega-Check Pocket (Neurtek S.A) meter. It was previously calibrated to non-ferrous basis by using the gauges supplied. The final dry film thickness (DFT) was $135 \pm 27 \mu\text{m}$. One single paint layer was applied in order to ensure reproducibility in the scratch hardness measurements.

Accelerated corrosion studies were carried out with both painted and non-painted samples. The test was performed using a patented equipment for cyclic test, developed at our laboratory [42–44]. The corrosion medium was an aqueous solution of NaCl (3.5 wt. %, pH = 6.6) stored in a glass container at room temperature. The operating cyclic conditions is described in our previous reported works [45,46]. Before testing, the samples were scribed and photographed with a digital camera. The total exposure time was 90 days for the painted specimens and 3 days (72 h) for the non-painted ones. ASTM D1654 standard was employed to evaluate the scribed area on painted specimens and optical microscopy was used to observe the epoxy coating delamination from the specimen cross-section sides.

For the non-painted samples, a computational image analysis technique was used for quantifying the corroded areas during the test [47]. This analysis was carried out, with

three repetitions, only with AA2024 substrates with Bare, DC and EAD treatments in order to have a direct comparison of the protection provided by such pretreatments.

The scratch tests were carried out with a CSM Revetest Scratch Tester (Anton Paar GmbH) with a Rockwell C tip of 200 μm radius. The measurement was performed with samples used in the abovementioned cyclic immersion test in order to evaluate coating adhesion and scratch resistance over time. The length of the scratch was 4 mm and the applied load was linearly incremented up to a force of 80 N. After the test, the specimens were visually inspected by optical microscopy (Dino-Lite AM3113T microscope, AnMo Electronics Corporation).

3. Results and Discussion

3.1. The Stability of ZrO_2 Nanocoating Comparing the DC and EAD Deposition Methods

It has been observed in a previous work that the potential applied for ZrO_2 electrodeposition influences the dry film thickness of the passivating layer, i.e., more negative potentials result in thicker films, whereas long deposition times are detrimental for good barrier layer formation [32,38]. Moreover, it has been observed that the film growth is fast in the first ten minutes of deposition, as recently pointed out by Milosev and co-workers for several types of Al alloys [48]. Unfortunately, for longer periods, pores and defects usually appear on the film and it hinders the oxide barrier protection properties. Based on such previous evidences, the ZrO_2 coatings were obtained after cathodic deposition at negative potential (-1.0 V) and after a constant electrodeposition time of 4 min. The coating thickness was measured by cross-section scanning electron microscopy images and varied depending on the substrate (31.1 ± 8.2 nm and 18.7 ± 4.0 nm, for AA1100 and AA2024, respectively) (Figure S1, supporting file). Those differences in the ZrO_2 coating thicknesses are associated to the presence of thick and stable Al_2O_3 and $\text{Al}(\text{OH})_3$ passivating layers in AA1100 grade after treatment with alkaline solutions (dissolution of $\text{Al}(\text{OH})_4^-$) and neutralization [49]. In AA2024 surfaces, the alkaline etching of Al surface prevents such thick structures in a certain way, due to the oxide/hydroxide enrichment with Cu compounds (dealloying process) in presence of basic solutions [50,51]. The detection of Al_2O_3 / AlOOH and Cu_2O and $\text{Cu}(\text{OH})_2$ compounds in AA1100 and AA2024, respectively, was already proved in our previous study [32].

Comparing EAD controlled ZrO_2 film formation with the classical chemical conversion coating method, the coating thickness on the latter is only dependent on ions diffusion. Therefore, it was slightly lower than that obtained from EAD method (24.9 ± 6.7 nm and 14.5 ± 4.1 nm, for AA1100 and AA2024, respectively). Additionally, topography SEM images evidenced that Zr-EAD process is able to cover the whole substrates with less apparent defects and less polishing marks visible than Zr-DC (Figure S1).

Figure 2 shows the polarization curves obtained with AA1100 substrate throughout 168 h (7 days) of exposure to the electrolyte.

From polarization curves of AA1100 substrates (Figure 2a–d), with progressive immersion time and after different pre-treatments, it is possible to note a pseudo-passivation region in the potential range of -1.0 V to 0 V, with the exception of Bare sample (Figure 2b). In pure aluminum alloy, due to the absence of noble intermetallic particles, there is a lack of local galvanic couples and it shows an enhanced passivity [21], which may be the reason for the more protective character of the non-coated specimens (Raw) observed in this alloy. Data obtained from the polarization curves shown in Figure 2 using the Tafel extrapolation method are presented in Table 1.

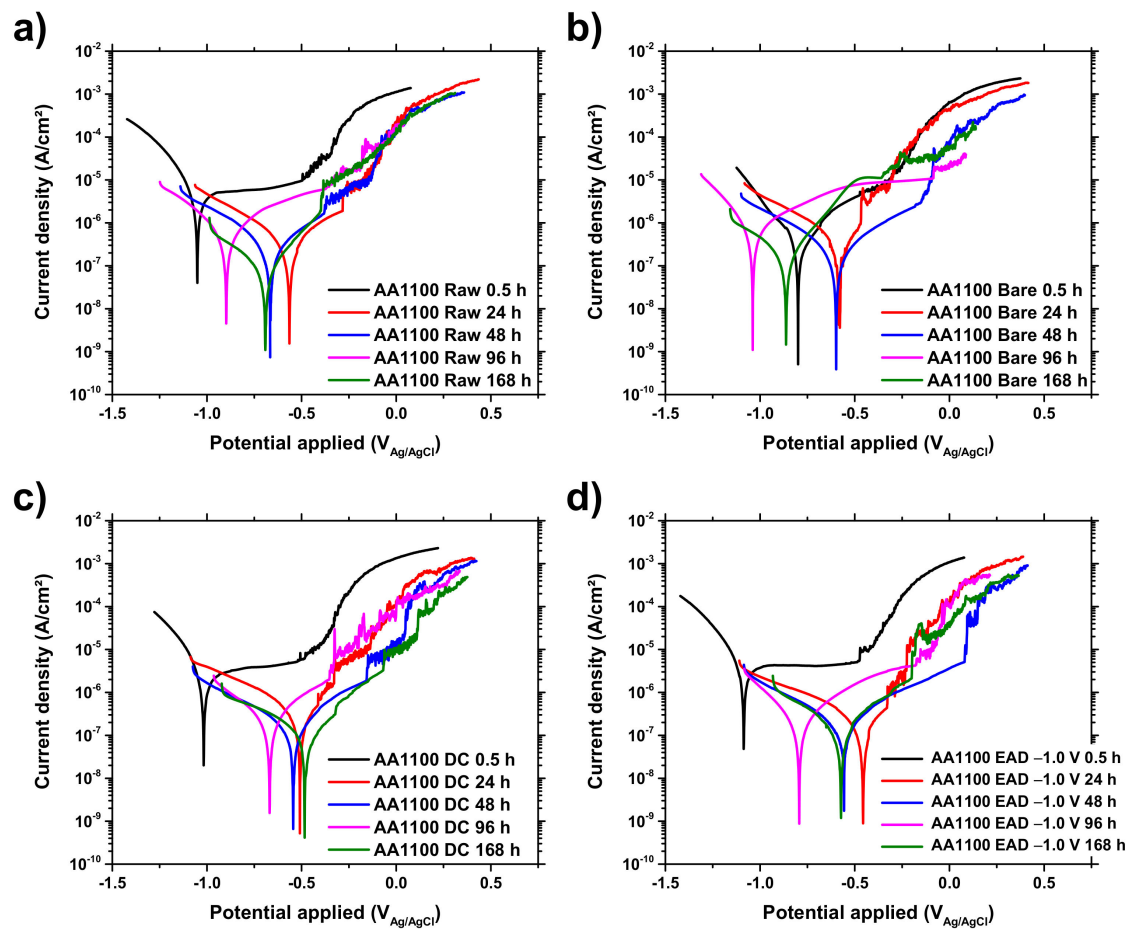


Figure 2. Polarization curves obtained for AA1100 specimens, throughout 168 h (7 days) of exposure in 0.05 M of NaCl solution, comparing the two methods used for the ZrO₂ metal deposition: (a) Raw, (b) Bare, (c) Dip-coating method, and (d) EAD method.

Table 1. Measured values of corrosion current density (j_{corr}), corrosion potential (E_{corr}) and breakdown potential (E_b) of AA1100 samples, during polarization tests with increased exposure time in 0.05 M NaCl solution.

Sample	Exposure Time (h)	j_{corr} (A/cm ²)	E_{corr} (V)	E_b (V)
AA1100 Raw	0.5	3.35×10^{-6}	-0.923	-0.495
	24	3.62×10^{-7}	-0.564	-0.283
	48	2.73×10^{-7}	-0.665	-0.380
	96	4.54×10^{-7}	-0.898	-0.353
	168	8.27×10^{-7}	-0.691	-0.397
AA1100 Bare	0.5	7.23×10^{-7}	-0.851	-
	24	4.34×10^{-7}	-0.585	-
	48	2.23×10^{-7}	-0.598	-0.152
	96	6.77×10^{-7}	-1.039	-0.084
AA1100 DC	168	1.68×10^{-7}	-0.862	-
	0.5	2.91×10^{-6}	-0.997	-0.492
	24	3.53×10^{-7}	-0.509	-
	48	1.59×10^{-7}	-0.544	-0.156
AA1100 EAD	96	2.13×10^{-7}	-0.668	-0.353
	168	9.08×10^{-8}	-0.484	-
	0.5	5.56×10^{-6}	-1.089	-0.461
	24	1.58×10^{-7}	-0.456	-
AA1100 EAD	48	1.80×10^{-7}	-0.557	+0.080
	96	1.77×10^{-7}	-0.793	-0.175
	168	1.50×10^{-7}	-0.573	-0.201

Note: All data were obtained by Tafel extrapolation, using Nova 2.1 software.

Although the corrosion potentials shift to high values in only 24 h, after 48 h of immersion, the pseudo-passivating layer found for Zr-EAD (Figure 2d) has higher breakdown potential (E_b) than that obtained for either Raw or DC samples (Figure 2a,c, respectively, and Table 1), showing better stability of the zirconium nanocoating promoted by the EAD method if compared to DC. After 96 h and 168 h such stability has been decreased, proving the poor barrier protection of ZrO_2 nanocoatings, generated by either DC or EAD methods. The E_b is supposed to be related to the penetration of chlorine ions across the ZrO_2 nanolayer, causing the displacement of the breakdown potential to more negative values. It is more evident on Bare plates, in which the interfacial porous and hygroscopic structure of $Al/Al(OH)_3$ layer plays a detrimental barrier effect if compared to Raw, DC and EAD samples.

Showing the effect of the surface treatment on another substrate, Figure 3 contains the polarization curves observed with AA2024 substrates in the same conditions as those of the AA1100 samples.

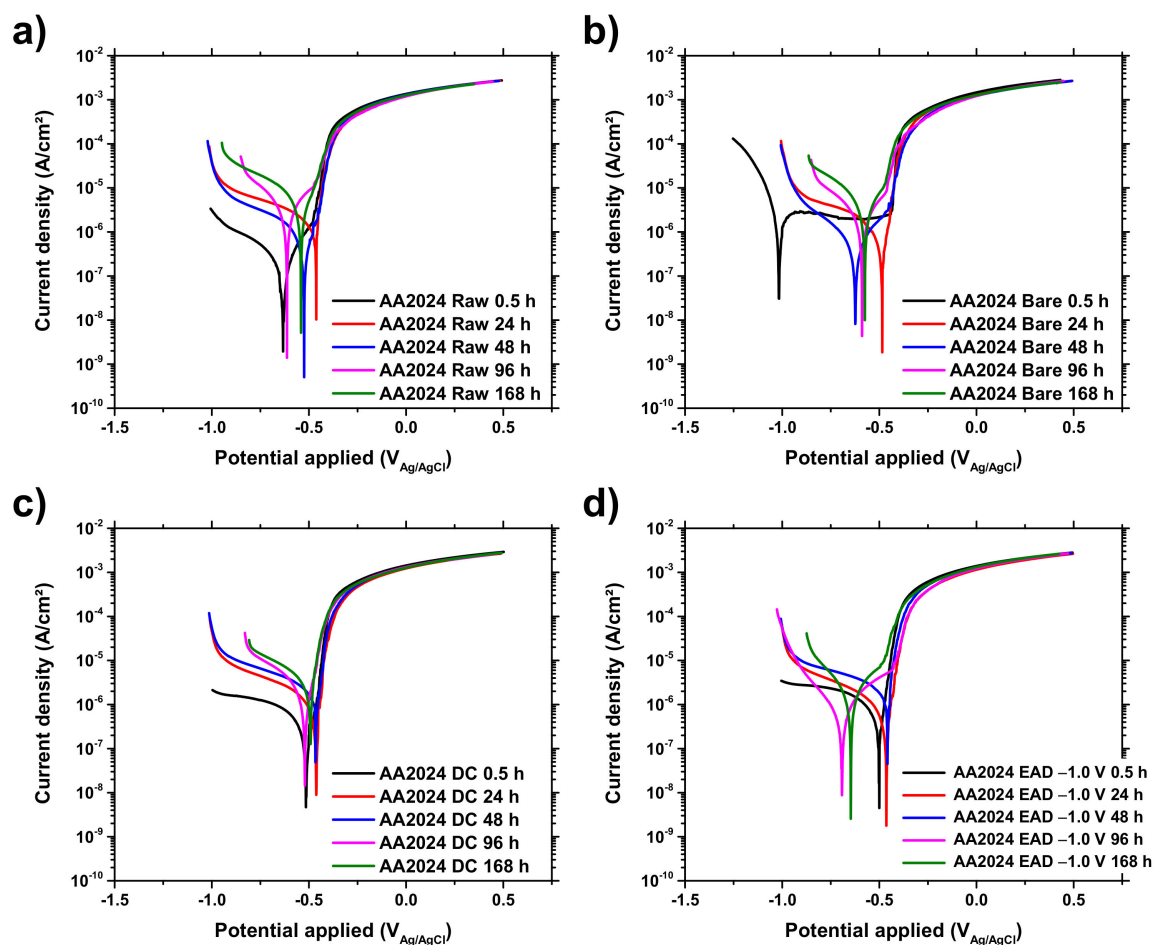


Figure 3. Polarization curves obtained for AA2024 specimens, throughout 168 h (7 days) of exposure in 0.05 M of NaCl solution, comparing the two methods used for the ZrO_2 metal deposition: (a) Raw, (b) Bare, (c) Dip-coating method, and (d) EAD method.

The Tafel extrapolation method was also carried out in the analysis of the AA2024 respective curves. The data obtained from such analysis is shown in Table 2.

Table 2. Measured values of corrosion current density (j_{corr}) and corrosion potential (E_{corr}) of AA2024 samples, during polarization tests with increased exposure time in 0.05 M NaCl solution.

Sample	Exposure Time (h)	j_{corr} (A/cm ²)	E_{corr} (V)
AA2024 Raw	0.5	4.52×10^{-7}	−0.576
	24	1.83×10^{-6}	−0.462
	48	1.10×10^{-6}	−0.525
	96	3.36×10^{-6}	−0.613
	168	5.12×10^{-6}	−0.541
AA2024 Bare	0.5	1.57×10^{-6}	−0.802 ¹
	24	1.37×10^{-6}	−0.485
	48	5.93×10^{-7}	−0.623
	96	2.15×10^{-6}	−0.589
	168	3.98×10^{-6}	−0.575
AA2024 DC	0.5	8.13×10^{-7}	−0.517
	24	1.33×10^{-6}	−0.462
	48	2.17×10^{-6}	−0.468
	96	2.31×10^{-6}	−0.520
	168	3.89×10^{-6}	−0.491
AA2024 EAD	0.5	9.77×10^{-7}	−0.575
	24	7.53×10^{-7}	−0.463
	48	2.21×10^{-6}	−0.458
	96	7.82×10^{-7}	−0.692
	168	1.74×10^{-6}	−0.647

Notes: All data were obtained by Tafel extrapolation, using Nova 2.1 software. ¹ The breakdown potential (E_b) found for this sample was −0.485 V.

As opposed to the observed in AA1100 specimens, AA2024 substrates do not present any pseudo-passive behavior (Figure 3) like that obtained for AA1100 panels, with exception of Bare sample at the initial immersion time (0.5 h, Figure 3b). However, the oxide/hydroxide Al layer is highly unstable and the anodic current increases sharply in only 24 h of sample exposition. From Figure 3d and Table 2, it is evident that AA2024 zirconium EAD specimens show lower anodic current density (j_{corr}), after 24 h of electrolyte immersion, if compared to the other specimens. This probably happens due to the better covering of intermetallic particles (Al_2CuMg , $\text{Cu}_3\text{Mn}_2\text{Al}$ and $\text{Al}_6(\text{Cu,Fe,Mn})$), such as that reported by Birbilis et al. [52]), caused by the ZrO_2 compact nanolayer, generated by controlled voltage application. The Cu-rich Al alloy is highly corrosion prone in Cl^- ion environment due to the presence of such compounds [53]. Fortunately, after 48 h of immersion time, the system stabilizes and j_{corr} of Zr-EAD/2024 disc shifts to more negative values compared to Raw plates (Figure S2). By contrary, the j_{corr} values enhanced gradually with immersion time for all the other samples, including Zr-DC. After 96 h of immersion, the anodic current density obtained for Zr-EAD on AA2024 plates is approximately one third of the one observed for DC. Therefore, we can conclude that the electrodeposition method produces films with better barrier properties over time. In Figure S2, the evolution of j_{corr} and E_{corr} are presented for comparison of the pre-treatments effects on both AA1100 and AA2024 substrates.

3.2. Porosity and Barrier Properties of Zr-EAD and Zr-CCC Coatings Evaluated by Potentiodynamic Polarization Curves, EIS Analysis and Accelerated Corrosion Test

Different methods can be used to approach the coatings' porosity. One of them is the polarization resistance, in which the porosity of a passivating layer is calculated from the electrical resistance of the substrate without and with the coat, according to the area in contact with the electrolyte, then the solution reaches the substrate through the open porosity across the coating. For the coating porosity analysis, the untreated and treated aluminum surfaces were compared using the polarization resistance data obtained for samples immersed during 24 h in NaCl solution (Equation (1) and Tables 1 and 2). The porosity values evidence that ZrO_2 generated by electrochemical method are more compact

(32.6% and 38.6%, for AA1100 and AA2024, respectively) than that obtained by adsorption chemical deposition (60.4% and 58.6%, for AA1100 and AA2024, respectively). These data being almost twice the porosity of Zr-EAD coatings. Another observation is that the metal composition does not affect the porosity of the ZrO₂ nanofilms. On the contrary, aluminum oxides and hydroxides formed after substrates degreasing in alkaline mixture (Bare) are highly porous (86.9%) in AA1100 if compared to AA2024 (41.5%). It is supported by the previous explanation about such oxides/hydroxides stability differences on both surfaces, mentioned in the Section 3.1.

After polarization studies, EIS measurements were performed to evaluate the Zr oxide-based coating barrier resistance, generated by DC and EAD techniques; comparing to the Raw and Bare samples. These results are enclosed in Tables 3 and 4.

Table 3. EIS data obtained for AA1100 substrates, after immersion in NaCl solution, from 0.5 h to 168 h of exposure time.

Sample Code	Exposure Time (h)	R _s (Ω cm ²)	R _p (Ω cm ²)	CPE _{dl} (F cm ⁻² s ⁿ⁻¹)	n _{CPE}
AA1100 Raw	0.5	349	6.2 × 10 ³	3.7 × 10 ⁻⁵	0.695
	24	346	7.3 × 10 ⁴	2.2 × 10 ⁻⁵	0.774
	48	353	20.6 × 10 ⁴	7.7 × 10 ⁻⁶	0.786
	96	354	21.8 × 10 ⁴	7.3 × 10 ⁻⁶	0.802
	168	331	15.1 × 10 ⁴	1.1 × 10 ⁻⁵	0.805
AA1100 Bare	0.5	349	9.9 × 10 ³	1.9 × 10 ⁻⁵	0.798
	24	331	7.6 × 10 ⁴	2.1 × 10 ⁻⁵	0.821
	48	353	17.3 × 10 ⁴	9.2 × 10 ⁻⁶	0.826
	96	324	10.9 × 10 ⁴	1.5 × 10 ⁻⁵	0.844
	168	356	7.7 × 10 ⁴	2.1 × 10 ⁻⁵	0.855
AA1100 DC	0.5	220	7.0 × 10 ⁴	2.1 × 10 ⁻⁵	0.792
	24	317	18.0 × 10 ⁴	8.8 × 10 ⁻⁶	0.816
	48	342	22.6 × 10 ⁴	7.0 × 10 ⁻⁶	0.804
	96	338	15.1 × 10 ⁴	1.1 × 10 ⁻⁵	0.817
	168	335	18.9 × 10 ⁴	8.4 × 10 ⁻⁶	0.821
AA1100 EAD	0.5	288	4.0 × 10 ⁴	2.4 × 10 ⁻⁵	0.779
	24	317	9.3 × 10 ⁴	1.7 × 10 ⁻⁵	0.790
	48	318	14.9 × 10 ⁴	1.1 × 10 ⁻⁵	0.785
	96	346	8.3 × 10 ⁴	1.9 × 10 ⁻⁵	0.847
	168	338	6.7 × 10 ⁴	1.9 × 10 ⁻⁵	0.851

Table 4. EIS data obtained for AA2024 substrates, after immersion in NaCl solution, from 0.5 h to 168 h of exposure time.

Sample Code	Exposure Time (h)	R _s (Ω cm ²)	R _p (Ω cm ²)	CPE _{dl} (F cm ⁻² s ⁿ⁻¹)	n _{CPE}
AA2024 Raw	0.5	389	5.6 × 10 ³	3.9 × 10 ⁻⁵	0.896
	24	335	4.6 × 10 ³	7.5 × 10 ⁻⁵	0.830
	48	379	6.1 × 10 ³	9.3 × 10 ⁻⁵	0.779
	96	373	4.2 × 10 ³	7.8 × 10 ⁻⁵	0.847
	168	365	2.3 × 10 ³	1.5 × 10 ⁻⁴	0.864
AA2024 Bare	0.5	363	2.3 × 10 ³	5.7 × 10 ⁻⁵	0.868
	24	358	3.4 × 10 ³	6.7 × 10 ⁻⁵	0.897
	48	364	4.0 × 10 ³	8.3 × 10 ⁻⁵	0.836
	96	368	3.4 × 10 ³	9.9 × 10 ⁻⁵	0.865
	168	368	2.8 × 10 ³	1.8 × 10 ⁻⁴	0.862
AA2024 DC	0.5	383	2.9 × 10 ⁴	1.4 × 10 ⁻⁵	0.855
	24	353	2.9 × 10 ³	6.0 × 10 ⁻⁵	0.864
	48	371	4.6 × 10 ³	1.3 × 10 ⁻⁴	0.844
	96	364	2.8 × 10 ³	1.4 × 10 ⁻⁴	0.860
	168	367	2.7 × 10 ³	2.1 × 10 ⁻⁴	0.855
AA2024 EAD	0.5	395	2.7 × 10 ⁴	2.7 × 10 ⁻⁵	0.890
	24	401	1.3 × 10 ⁴	3.5 × 10 ⁻⁵	0.856
	48	392	9.7 × 10 ³	8.4 × 10 ⁻⁵	0.804
	96	360	7.6 × 10 ³	1.7 × 10 ⁻⁴	0.817
	168	371	4.5 × 10 ³	1.9 × 10 ⁻⁴	0.833

This approach was first carried out without the epoxy coating bilayer system. The Nyquist and Bode plots were evaluated after 24, 48, 96 and 168 h of samples immersion in the aggressive medium. A comparison between the polarization resistance values of all samples is displayed in Figure 4.

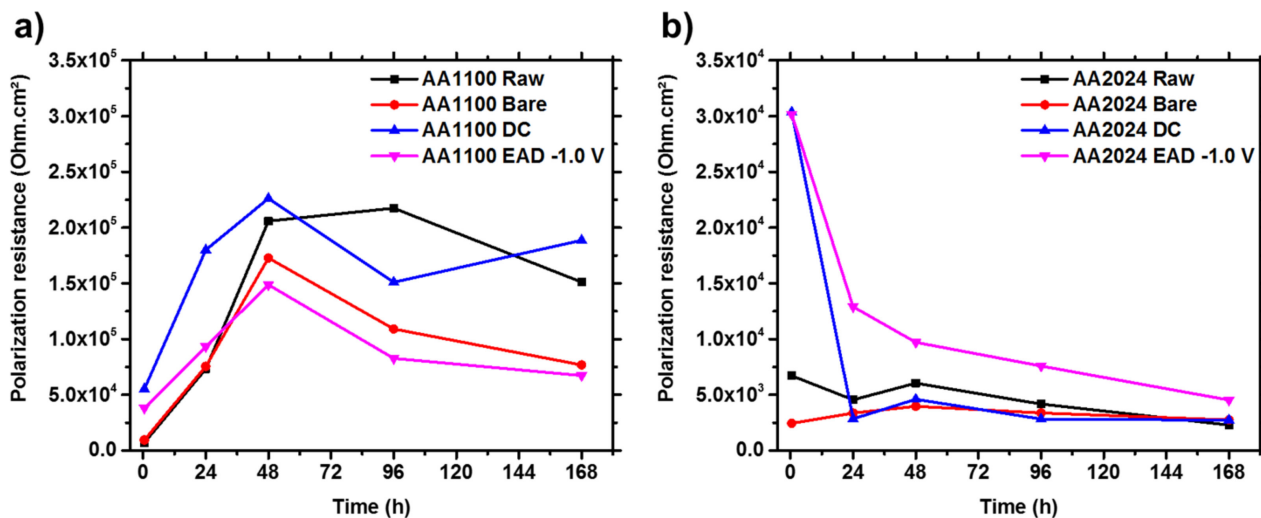


Figure 4. Polarization resistances of AA1100 and AA2024 samples, with increasing immersion time in NaCl solution (0.05 M).

As can be seen in Figure 4, the polarization resistance (R_p), which is associated to the porous oxide interface between the metal substrate and the electrolyte solution as well as to the charge transfer resistance of the coating, has opposite trend in pure Al and Cu-rich surfaces. The R_p gradually raises until 48 h (Figure 4a) indicating a passivating ability in AA1100. However, this effect is not stable over time and the observed fluctuations after this time demonstrate the instability of the oxide coatings ($\text{Al}_2\text{O}_3/\text{AlOOH}$ and ZrO_2 , in Raw/Bare and DC/EAD samples, respectively). On the other hand, the trend observed for R_p of AA2024 surfaces (Figure 4b), shows that the Zr-EAD coating loses its barrier protection more gradually than Zr-DC sample, which rapidly achieves a plateau of low resistance value in only 24 h. The slowest decay of R_p in Zr-EAD layer on AA2024 can be explained due to the presence of less defects if compared to the chemical conversion coating induced by ions diffusion in Zr-DC method. The comparatively higher values of R_p found in DC and EAD conversion coatings with respect to Raw and Bare samples in AA2024 at initial time (0.5 h, Table 4) is due to the well-covered intermetallic sites enriched in copper alloying composition, which favours the preferential nucleation of zirconium compounds, as stated previously in several works [6,14,54].

For simplification, the most relevant plots of Nyquist and Bode curves (24 h and 168 h) are showed in the supporting file (Figures S3 and S4, for AA1100 and AA2024 samples, respectively), as well as a deeper discussion on the impedance data.

Another possible approach for the comparison of the different treatments throughout the exposure time is the analysis of the impedance module $|Z|$ at low frequencies, which is proportionally related to the corrosion resistance [21,55]. Such comparison is shown in Figure S5. The results evidenced similar conclusions as that found with the R_p analysis.

Such results support the data of porosity calculated by the polarization resistance study for coatings with 24 h of salt solution immersion, i.e., higher porosity implies lower barrier protection.

In order to have a direct comparison between the most relevant pretreatments in this study on AA2024 substrates, a cyclic accelerated corrosion test was performed with AA2024 Bare, AA2024 DC and AA2024 EAD non-painted specimens. Figure 5 shows the evolution of the corroded areas during the test.

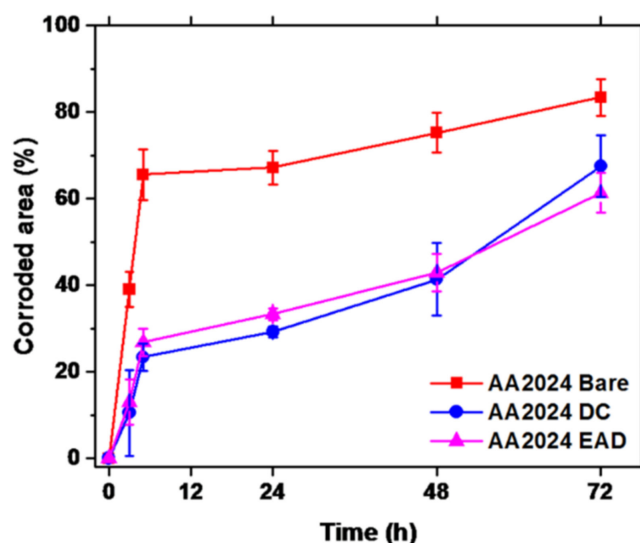


Figure 5. Measured corroded areas during 72 h of cyclic accelerated corrosion test with non-painted AA2024 substrates.

A sharp increase in the corroded area was observed for all samples during the first 5 h of the test, after which a less pronounced increase is noticed until the end of the test. Despite also presenting visible corrosion products after only 5 h of exposure, the corroded areas of the Zr-coated samples (DC and EAD) are consistently smaller than the ones observed in Bare samples throughout the entire test, being approximately half of it after 5 h. During the tested period both DC and EAD had similar results, which indicates that the differences observed between these two methods do not lead to significant changes in the barrier protection in an aggressive environment. Given the nanometric thickness of the films and their porosities, this result is in agreement with the previous observations. Photographs of representative specimens that underwent this test are available in Figure S6.

The presence of corrosion products in such a short test confirms that the corrosion protection provided by the Zr-based nanocoating is not enough for it to act as a final barrier layer, as the progressive penetration of chlorine ions leads to the barrier destruction and a further layer of organic impermeable coating is urged. Even in conditions where the native oxide layer provides more barrier protection, the zirconium conversion coating use can be seen as an effective solution for the subsequent deposition of organic coatings, as stated previously [6,11,23]. Thus, the ZrO₂ nanocoating effect in the promotion of organic coatings adherence will be discussed in the next section.

3.3. Evaluation of the Dual Protected Aluminum Substrates under Prolonged Exposition to NaCl Solution

Accelerated corrosion test was carried out in an automated robot and in a more aggressive environment (NaCl 3.5 wt. %) if compared to previous electrochemical studies (NaCl 0.05 M, 2.92 wt. %). The samples were extracted every 30 days, until completing 90 days of testing. Taking into account that the best results of zirconium oxide layer (good homogeneity and compactness observed by polarization and SEM analyses) were obtained with the EAD method, it was the process tried for the deposition of an additional barrier coat. Bare substrates (*i.e.*, degreased AA1100 and AA2024 substrates) were chosen for comparison with the Zr-EAD samples, due to the worst case of such interface composed mainly by Al₂O₃ and hydroxide compounds. Figure S7 includes the photographs of plates and discs used for this assay. Cross-section SEM images of the samples submitted to this test are shown in Figure 6.

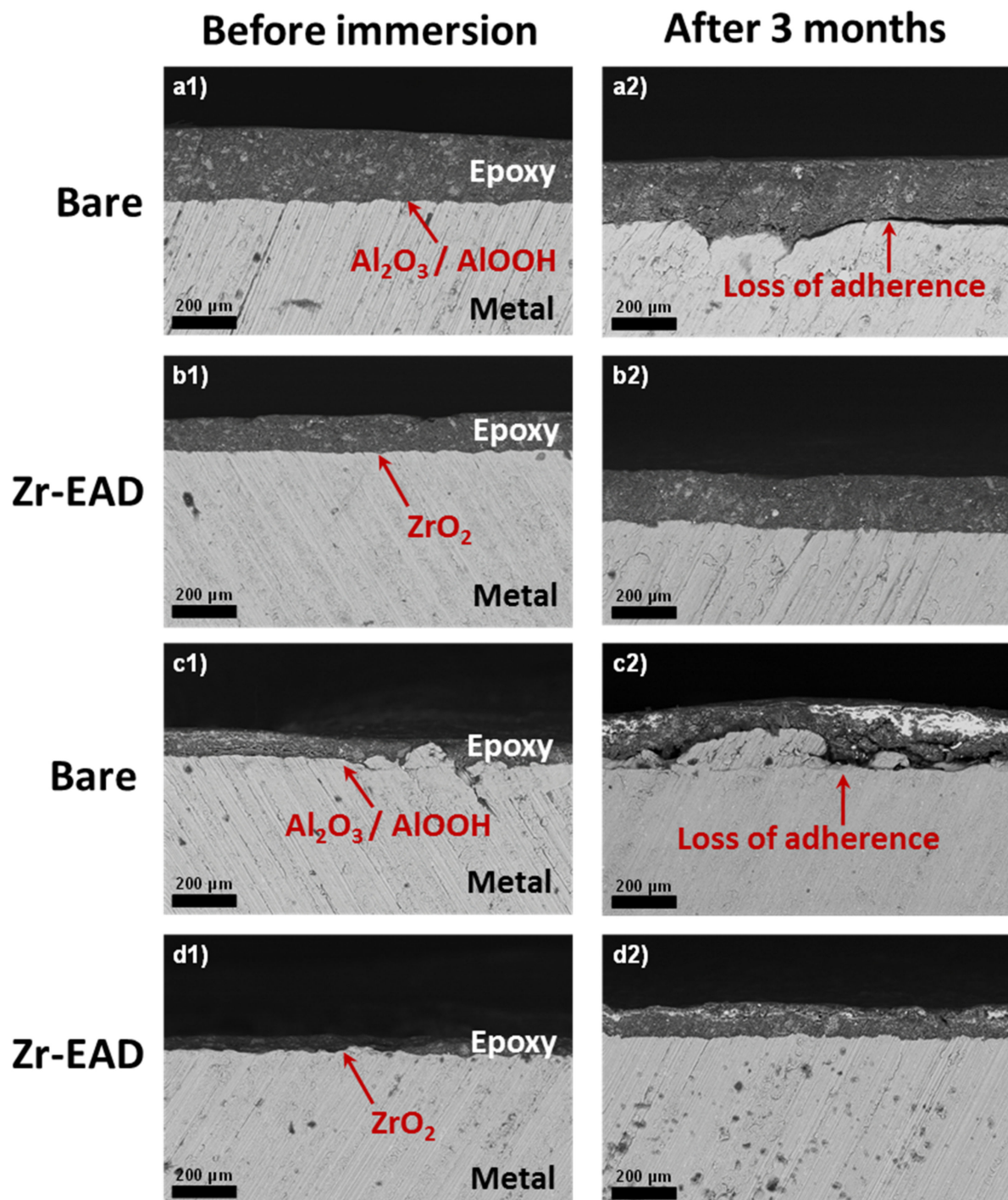


Figure 6. Cross-section SEM images of the following specimens: (a) AA1100 Bare, (b) AA1100 EAD, (c) AA2024 Bare and (d) AA2024 EAD; before (1) and after (2) 90 days of cyclic immersion corrosion test in NaCl 3.5 wt. %.

Although paint delamination or blistering were not observed during the accelerated corrosion test in the macroscopic images, microscopic observation of the metal/primer interface (Figure 6) revealed a noticeable loss of organic coating adherence in Bare samples (Figure 6(a2,c2)). On the contrary, the presence of Zr-EAD avoided the organic coating delamination (Figure 6(b2,d2)). This observation indicates that the pre-treatment induced by EAD method efficiently maintains the protection of either AA1100 or AA2024 alloys throughout extended exposition periods, which is a fundamental requirement for its use as a pre-treatment for the application of organic topcoats.

Figure 6 shows only non-scribed zones. Additional cross section optical microscopy images from scribed area, of both Bare and EAD samples coated with epoxy primer, are presented in Figure S8. It is observable that in all Zr-EAD specimens the paint adherence is not limited to the area far from the defect but also in the scribed mark surrounding, where the formation of corrosion products usually promotes the paint delamination. Altogether proves that zirconium oxide conversion coatings are a useful pre-treatment to potentiate the integrity of the metal/primer interface, even in structural alloys, like AA2024, that is more prone to corrosion due to the presence of Cu-rich intermetallics.

3.4. Scratch Testing

Scratch tests did not produce a clear delamination difference between Bare/epoxy coating and Zr-EAD/epoxy coating in AA1100 samples. However, detailed inspection of the deformation produced by scratching in AA2024/epoxy material revealed relevant differences. Figure 7 contains optical microscopy images of two relevant samples used in this test.

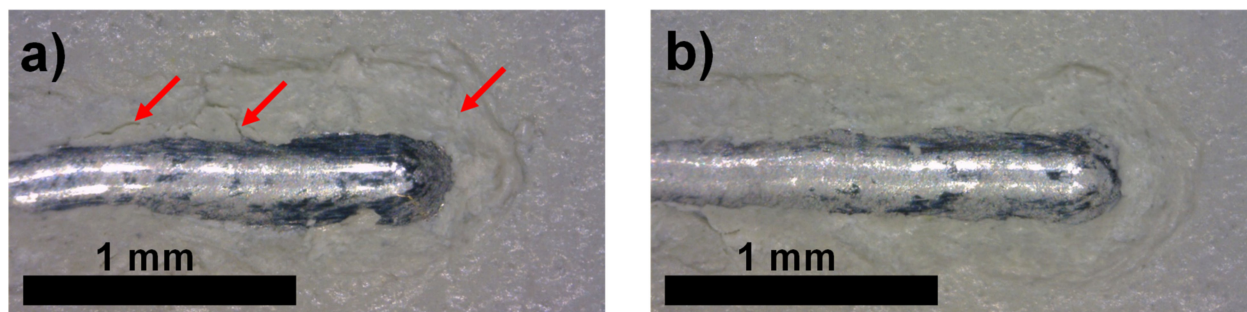


Figure 7. Optical microscopy images of the scratch zone, produced after indentation test of AA2024 specimens, under 90 days of cyclic immersion corrosion test in 3.5 wt. % NaCl. (a) AA2024 Bare/epoxy coating and (b) AA2024 Zr-EAD/epoxy coating. Red arrows indicate microcracking zones.

In Figure 7, the mark produced in the scratch test of AA2024 specimens after 90 days of cyclic immersion test is presented. The abovementioned loss of adhesion in Bare samples may have been initiated in small defects or irregularities present on the Al oxide/hydroxide interface. Careful inspection of the image shown in Figure 7a reveals that the organic coating is also microcracked, which implies that, not only it loses adhesion after immersion, but also the structural integrity of the epoxy coating as well. Moreover, Zr-EAD/epoxy coating (Figure 7b), in contrast, presents a good adhesion and with no visible microcracking after immersion, indicating that the mechanical performance on service is better than the Bare pre-treatment [23].

4. Conclusions

In this work, AA1100 surfaces containing ZrO₂ nanocoatings proved to have high instability of its native oxide/hydroxide interface layer, in long exposition time, than that of AA2024 structural alloy. Although the Zr-based nanocoatings are porous, the presence of such nanometric zirconium oxide film is still beneficial for both substrates if compared to the aluminum surface uniquely ground or degreased with alkaline solution.

The low barrier property of the zirconium oxide films was overcome by the application of a further layer of an anticorrosive organic coating. The long-term accelerated corrosion tests and the scratch assays demonstrated the superior adherence of samples with an ultra-thin layer of ZrO₂, generated by electro-assisted technique, if compared to samples with the chemical conversion treatment, due to the lower porosity found for the first. The dual system is able to maintain the integrity of the metal surface and the coating adherence as long as 90 days, whereas samples without Zr-based nanocoatings cannot do. All together represents an alternative to chromate and phosphating processes which have several

environmental problems related to the toxicity of chemical baths and to the large amount of waste generation.

Supplementary Materials: The following are available online at <https://www.mdpi.com/article/10.3390/su13179688/s1>, Figure S1: Topography SEM images of: (a) AA1100/Zr-DC coating; (b) AA1100/Zr-EAD coating; (c) AA2024/Zr-DC coating; and (d) AA2024/Zr-EAD coating. The insets on (b) and (d) images represent the cross-cut of those sample surfaces (by focused ion beam), used for the thicknesses measurements, Figure S2: Corrosion current densities (J_{corr}) measured on: (a) AA1100 and (b) AA2024 substrates; and corrosion potentials (E_{corr}) measured on: (c) AA1100 and (d) AA2024 treated specimens. The values correspond to the Tafel extrapolation of the polarization curves obtained during the exposure of the analyzed samples to a NaCl 0.05 M electrolyte, throughout 168 h (7 days), Figure S3: Nyquist (1) and Bode (2) diagrams obtained from electrochemical impedance spectroscopy tests of AA1100 pre-treated samples, after: (a) 24 h and (b) 168 h of exposure to the electrolyte solution, Figure S4: Nyquist (1) and Bode (2) diagrams obtained from electrochemical impedance spectroscopy tests of AA2024 pre-treated samples after: (a) 24 h and (b) 168 h of exposure to the electrolyte solution, Figure S5: Impedance modules $|Z|$ at 0.1 Hz, measured through electrochemical impedance spectroscopy, from 0.5 to 168 h of immersion in NaCl 0.05 M solution: (a) AA1100 and (b) AA2024 substrates, with different pre-treatments, Figure S6: Photographs of AA2024 specimens submitted to cyclic accelerated corrosion test during 72 h, Figure S7: Digital photographs of AA1100 plates (a) and AA2024 discs (b), before and after 90 days of accelerated corrosion assays (NaCl 3.5 wt.%) and Figure S8: Optical microscopy images of the cross-section of scribed areas in: (a) AA1100 and (b) AA2024 specimens, submitted to accelerated corrosion test during 90 days.

Author Contributions: Conceptualization, V.B.M., A.M. and E.A.; methodology, V.B.M. and E.A.; validation, V.B.M. and E.A.; formal analysis, V.B.M., E.J.-P. and E.A.; investigation, V.B.M. and E.A.; resources, C.A.; data curation, V.B.M.; writing—original draft preparation, E.A.; writing—review and editing, all authors; supervision, A.M. and E.A.; project administration, E.A. and C.A.; funding acquisition, C.A. All authors have read and agreed to the published version of the manuscript.

Funding: This work has been supported by MINECO and FEDER funds (RTI2018-098951-B-I00, PGC2018-096855-B-C41) and by Generalitat de Catalunya (2017SGR359). V.B.M. received funding from Conselho Nacional de Desenvolvimento Científico e Tecnológico (CNPq, No. 200890/2018-2 and No. 142042/2017-0) and Coordenação de Aperfeiçoamento de Pessoal de Nível Superior (CAPES, No. 88881.188990/2018-01).

Data Availability Statement: The data supporting reported results can be supplied by the authors upon request.

Conflicts of Interest: The authors declare no conflict of interest.

References

1. Narayanan, T.S.N.S. Surface pretreatment by phosphate conversion coatings—A review. *Rev. Adv. Mater. Sci.* **2005**, *9*, 130–177.
2. Velasquez, C.S.; Pimenta, E.P.S.; Lins, V.F.C. Anticorrosive Behavior and Porosity of Tricationic Phosphate and Zirconium Conversion Coating on Galvanized Steel. *J. Mater. Eng. Perform.* **2018**, *27*, 2138–2147. [[CrossRef](#)]
3. European Parliament and of the Council. *Regulation (EC) No 1907/2006—Registration, Evaluation, Authorisation and Restriction of Chemicals (REACH)*; European Parliament and of the Council: Strasbourg, France, 2006.
4. Becker, M. Chromate-free chemical conversion coatings for aluminum alloys. *Corros. Rev.* **2019**, *37*, 321–342. [[CrossRef](#)]
5. Gharbi, O.; Thomas, S.; Smith, C.; Birbilis, N. Chromate replacement: What does the future hold? *Mater. Degrad.* **2018**, *2*, 23–25. [[CrossRef](#)]
6. Milošev, I.; Frankel, G.S. Conversion Coatings Based on Zirconium and/or Titanium. *J. Electrochem. Soc.* **2018**, *165*, C127–C144. [[CrossRef](#)]
7. Doerre, M.; Hibbitts, L.; Patrick, G.; Akafuah, N. Advances in Automotive Conversion Coatings during Pretreatment of the Body Structure: A Review. *Coatings* **2018**, *8*, 405. [[CrossRef](#)]
8. Yoganandan, G.; Premkumar, K.P.; Balaraju, J.N. Evaluation of corrosion resistance and self-healing behavior of zirconium–cerium conversion coating developed on AA2024 alloy. *Surf. Coatings Technol.* **2015**, *270*, 249–258. [[CrossRef](#)]
9. Asemanni, H.R.; Ahmadi, P.; Sarabi, A.A.; Mohammadloo, H.E. Effect of zirconium conversion coating: Adhesion and anti-corrosion properties of epoxy organic coating containing zinc aluminum polyphosphate (ZAPP) pigment on carbon mild steel. *Prog. Org. Coat.* **2016**, *94*, 18–27. [[CrossRef](#)]

10. Liu, Y.; Yang, Y.; Zhang, C.; Zhang, T.; Yu, B.; Meng, G.; Shao, Y.; Wang, F.; Liu, L. Protection of AA5083 by a Zirconium-Based Conversion Coating. *J. Electrochem. Soc.* **2016**, *163*, C576–C586. [[CrossRef](#)]
11. Fockaert, L.I.; Taheri, P.; Abrahams, S.T.; Boelen, B.; Terryn, H.; Mol, J.M.C. Zirconium-based conversion film formation on zinc, aluminium and magnesium oxides and their interactions with functionalized molecules. *Appl. Surf. Sci.* **2017**, *423*, 817–828. [[CrossRef](#)]
12. Cerezo, J.; Taheri, P.; Vandendael, I.; Posner, R.; Lill, K.; de Wit, J.H.W.; Mol, J.M.C.; Terryn, H. Influence of surface hydroxyls on the formation of Zr-based conversion coatings on AA6014 aluminum alloy. *Surf. Coat. Technol.* **2014**, *254*, 277–283. [[CrossRef](#)]
13. George, F.O.; Skeldon, P.; Thompson, G.E. Formation of zirconium-based conversion coatings on aluminium and Al–Cu alloys. *Corros. Sci.* **2012**, *65*, 231–237. [[CrossRef](#)]
14. Sarfraz, A.; Posner, R.; Lange, M.M.; Lill, K.; Erbe, A. Role of Intermetallics and Copper in the Deposition of ZrO₂ Conversion Coatings on AA6014. *J. Electrochem. Soc.* **2014**, *161*, C509–C516. [[CrossRef](#)]
15. Adhikari, S.; Unocic, K.A.; Zhai, Y.; Frankel, G.S.; Zimmerman, J.; Fristad, W. Hexafluorozirconic acid based surface pretreatments: Characterization and performance assessment. *Electrochim. Acta* **2011**, *56*, 1912–1924. [[CrossRef](#)]
16. Liu, X.; Vonk, D.; Jiang, H.; Kisslinger, K.; Tong, X.; Ge, M.; Nazaretski, E.; Ravel, B.; Foster, K.; Petrash, S.; et al. Environmentally Friendly Zr-Based Conversion Nanocoatings for Corrosion Inhibition of Metal Surfaces Evaluated by Multimodal X-ray Analysis. *ACS Appl. Nano Mater.* **2019**, *2*, 1920–1929. [[CrossRef](#)]
17. Li, L.; Desouza, A.L.; Swain, G.M. In situ pH measurement during the formation of conversion coatings on an aluminum alloy (AA2024). *Analyst* **2013**, *138*, 4398. [[CrossRef](#)] [[PubMed](#)]
18. Fockaert, L.I.; Ankora, M.V.E.; Van Dam, J.P.B.; Pletincx, S.; Yilmaz, A.; Boelen, B.; Hauffman, T.; Garcia-Gonzalez, Y.; Terryn, H.; Mol, J.M.C. Effect of organic additives in fluoacid-based Ti and Zr-treatments for galvanized steel on the stability of a polymer coated interface. *Prog. Org. Coatings* **2020**, *146*, 105738. [[CrossRef](#)]
19. Pinheiro, J.S.; Regio, G.; Cardoso, H.R.P.; Oliveira, C.T.; Ferreira, J.Z. Influence of Concentration and pH of Hexafluorozirconic Acid on Corrosion Resistance of Anodized AA7075-T6. *Mater. Res.* **2019**, *22*, 1–11. [[CrossRef](#)]
20. Cardoso, H.R.P.; Rapacki, C.; Ferreira, J.Z. Monitoring of a Zr-based conversion coating on galvanised steel and its performance against corrosion. *Corros. Eng. Sci. Technol.* **2019**, *54*, 726–730. [[CrossRef](#)]
21. Šekularac, G.; Kovač, J.; Milošev, I. Prolonged protection, by zirconium conversion coatings, of AlSi7Mg0.3 aluminium alloy in chloride solution. *Corros. Sci.* **2020**, *169*, 108615. [[CrossRef](#)]
22. Van Dam, J.P.B.; Abrahams, S.T.; Yilmaz, A.; Gonzalez-Garcia, Y.; Terryn, H.; Mol, J.M.C. Effect of surface roughness and chemistry on the adhesion and durability of a steel-epoxy adhesive interface. *Int. J. Adhes. Adhes.* **2020**, *96*, 102450. [[CrossRef](#)]
23. Fockaert, L.I.; Pletincx, S.; Ganzinga-Jurg, D.; Boelen, B.; Hauffman, T.; Terryn, H.; Mol, J.M.C. Chemisorption of polyester coatings on zirconium-based conversion coated multi-metal substrates and their stability in aqueous environment. *Appl. Surf. Sci.* **2020**, *508*, 144771. [[CrossRef](#)]
24. Mohammadloo, H.E.; Sarabi, A.A.; Hosseini, R.M.; Sarayloo, M.; Sameie, H.; Salimi, R. A comprehensive study of the green hexafluorozirconic acid-based conversion coating. *Prog. Org. Coat.* **2014**, *77*, 322–330. [[CrossRef](#)]
25. Lostak, T.; Krebs, S.; Maljusch, A.; Gothe, T.; Giza, M.; Kimpel, M.; Flock, J.; Schulz, S. Formation and characterization of Fe³⁺/Cu²⁺-modified zirconium oxide conversion layers on zinc alloy coated steel sheets. *Electrochim. Acta* **2013**, *112*, 14–23. [[CrossRef](#)]
26. Ghanbari, A.; Attar, M.M. Surface free energy characterization and adhesion performance of mild steel treated based on zirconium conversion coating: A comparative study. *Surf. Coatings Technol.* **2014**, *246*, 26–33. [[CrossRef](#)]
27. Sababi, M.; Terryn, H.; Mol, J.M.C. The influence of a Zr-based conversion treatment on interfacial bonding strength and stability of epoxy coated carbon steel. *Prog. Org. Coat.* **2017**, *105*, 29–36. [[CrossRef](#)]
28. Taheri, P.; Laha, P.; Terryn, H.; Mol, J.M.C. An in situ study of zirconium-based conversion treatment on zinc surfaces. *Appl. Surf. Sci.* **2015**, *356*, 837–843. [[CrossRef](#)]
29. Reck, J.; Wang, Y.-M.; Kuo, H.-H.H. Development of Zirconium-based Conversion Coatings for the Pretreatment of AZ91D Magnesium Alloy Prior to Electrocoating. In *Magnesium Technology 2011*; Sillekens, W.H., Agnew, S.R., Neelameggham, N.R., Mathaudhu, S.N., Eds.; Springer International Publishing: Cham, Switzerland, 2011; pp. 523–529, ISBN 978-3-319-48568-3.
30. Andreatta, F.; Paussa, L.; Lanzutti, A.; Navarro, N.C.R.; Aparicio, M.; Castro, Y.; Duran, A.; Ondratschek, D.; Fedrizzi, L. Development and industrial scale-up of ZrO₂ coatings and hybrid organic–inorganic coatings used as pre-treatments before painting aluminium alloys. *Prog. Org. Coat.* **2011**, *72*, 3–14. [[CrossRef](#)]
31. Coloma, P.S.; Izagirre, U.; Belaustegi, Y.; Jorcin, J.B.; Cano, F.J.; Lapeña, N. Chromium-free conversion coatings based on inorganic salts (Zr/Ti/Mn/Mo) for aluminum alloys used in aircraft applications. *Appl. Surf. Sci.* **2015**, *345*, 24–35. [[CrossRef](#)]
32. Moreira, V.B.; Puiggali-Jou, A.; Jiménez-Piqué, E.; Alemán, C.; Meneguzzi, A.; Armelin, E. Green nanocoatings based on the deposition of zirconium oxide: The role of the substrate. *Materials* **2021**, *14*, 1043. [[CrossRef](#)]
33. Dong, X.; Argekar, S.; Wang, P.; Schaefer, D.W. In situ Evolution of Trivalent Chromium Process Passive Film on Al in a Corrosive Aqueous Environment. *ACS Appl. Mater. Interfaces* **2011**, *3*, 4206–4214. [[CrossRef](#)] [[PubMed](#)]
34. Chaim, R.; Silberman, I.; Gal-Or, L. Electrolytic ZrO₂ Coatings II: Microstructural aspects. *J. Electrochem. Soc.* **1991**, *138*, 1942. [[CrossRef](#)]
35. Gal-Or, L.; Silberman, I.; Chaim, R. Electrolytic ZrO₂: I. Electrochemical aspects. *J. Electrochem. Soc.* **1991**, *138*, 1939. [[CrossRef](#)]

36. Yen, S.K. Characterization of Electrolytic ZrO₂ Coating on AISI 316L Stainless Steel. *J. Electrochem. Soc.* **1999**, *146*, 1392–1396. [[CrossRef](#)]
37. Yen, S.; Guo, M.; Zan, H. Characterization of electrolytic ZrO₂ coating on Co–Cr–Mo implant alloys of hip prosthesis. *Biomaterials* **2001**, *22*, 125–133. [[CrossRef](#)]
38. Shacham, R.; Mandler, D.; Avnir, D. Electrochemically Induced Sol–Gel Deposition of Zirconia Thin Films. *Chem. Eur. J.* **2004**, *10*, 1936–1943. [[CrossRef](#)] [[PubMed](#)]
39. Liu, L.; Mandler, D. Electrochemical Deposition of Sol–Gel Films. In *Handbook of Sol–Gel Science and Technology*; Springer International Publishing: Cham, Switzerland, 2018; pp. 531–568.
40. Creus, J.; Mazille, H.; Idrissi, H. Porosity evaluation of protective coatings onto steel, through electrochemical techniques. *Surf. Coatings Technol.* **2000**, *130*, 224–232. [[CrossRef](#)]
41. Chai, Z.; Li, J.; Lu, X.; He, D. Use of electrochemical measurements to investigate the porosity of ultra-thin Al₂O₃ films prepared by atomic layer deposition. *RSC Adv.* **2014**, *4*, 39365–39371. [[CrossRef](#)]
42. Liesa, F.; Alemán, C.; Iribarren, J.I. Brazo Mecánico para Realizar Ensayos de Corrosión Acelerados. Patent P200500895, 12 April 2005.
43. Ocampo, C.; Armelin, E.; Liesa, F.; Alemán, C.; Ramis, X.; Iribarren, J.I. Application of a polythiophene derivative as anticorrosive additive for paints. *Prog. Org. Coat.* **2005**, *53*, 217–224. [[CrossRef](#)]
44. Liesa, F.; Ocampo, C.; Alemán, C.; Armelin, E.; Oliver, R.; Estrany, F. Application of electrochemically produced and oxidized poly(3,4-ethylenedioxythiophene) as anticorrosive additive for paints: Influence of the doping level. *J. Appl. Polym. Sci.* **2006**, *102*, 1592–1599. [[CrossRef](#)]
45. Armelin, E.; Pla, R.; Liesa, F.; Ramis, X.; Iribarren, J.I.; Alemán, C. Corrosion protection with polyaniline and polypyrrole as anticorrosive additives for epoxy paint. *Corros. Sci.* **2008**, *50*, 721–728. [[CrossRef](#)]
46. Iribarren-Mateos, J.I.; Buj-Corral, I.; Vivancos-Calvet, J.; Alemán, C.; Iribarren, J.I.; Armelin, E. Silane and epoxy coatings: A bilayer system to protect AA2024 alloy. *Prog. Org. Coat.* **2015**, *81*, 47–57. [[CrossRef](#)]
47. Moreira, V.B.; Krummenauer, A.; Ferreira, J.Z.; Veit, H.M.; Armelin, E.; Meneguzzi, A. Computational image analysis as an alternative tool for the evaluation of corrosion in salt spray test. *Stud. Univ. Babeş Bolyai Chem.* **2020**, *65*, 45–61.
48. Šekularac, G.; Kovač, J.; Milošev, I. Comparison of the Electrochemical Behaviour and Self-sealing of Zirconium Conversion Coatings Applied on Aluminium Alloys of series 1xxx to 7xxx. *J. Electrochem. Soc.* **2020**, *167*, 111506. [[CrossRef](#)]
49. Boukerche, I.; Djerad, S.; Benmansour, L.; Tifouti, L.; Saleh, K. Degradability of aluminum in acidic and alkaline solutions. *Corros. Sci.* **2014**, *78*, 343–352. [[CrossRef](#)]
50. de Frutos, A.; Arenas, M.A.; Liu, Y.; Skeldon, P.; Thompson, G.E.; de Damborenea, J.; Conde, A. Influence of pre-treatments in cerium conversion treatment of AA2024-T3 and 7075-T6 alloys. *Surf. Coat. Technol.* **2008**, *202*, 3797–3807. [[CrossRef](#)]
51. Li, L.; Desouza, A.L.; Swain, G.M. Effect of Deoxidation Pretreatment on the Corrosion Inhibition Provided by a Trivalent Chromium Process (TCP) Conversion Coating on AA2024-T3. *J. Electrochem. Soc.* **2014**, *161*, C246–C253. [[CrossRef](#)]
52. Šekularac, G.; Milošev, I. Electrochemical Behavior and Self-Sealing Ability of Zirconium Conversion Coating Applied on Aluminum Alloy 3005 in 0.5 M NaCl Solution. *J. Electrochem. Soc.* **2020**, *167*, 021509. [[CrossRef](#)]
53. Birbilis, N.; Zhu, Y.M.; Kairy, S.K.; Glenn, M.A.; Nie, J.F.; Morton, A.J.; Gonzalez-Garcia, Y.; Terryn, H.; Mol, J.M.C.; Hughes, A.E. A closer look at constituent induced localised corrosion in Al–Cu–Mg alloys. *Corros. Sci.* **2016**, *113*, 160–171. [[CrossRef](#)]
54. Torras, J.; Azambuja, D.S.; Wolf, J.M.; Alemán, C.; Armelin, E. How organophosphonic acid promotes silane deposition onto aluminum surface: A detailed investigation on adsorption mechanism. *J. Phys. Chem. C* **2014**, *118*, 17724–17736. [[CrossRef](#)]
55. Lunder, O.; Simensen, C.; Yu, Y.; Nisancioglu, K. Formation and characterisation of Ti–Zr based conversion layers on AA6060 aluminium. *Surf. Coat. Technol.* **2004**, *184*, 278–290. [[CrossRef](#)]